Journal of Atmospheric and Solar-Terrestrial Physics 171 (2018) 201–209

Contents lists available at ScienceDirect

Journal of Atmospheric and Solar-Terrestrial Physics

journal homepage: www.elsevier.com/locate/jastp

Comparisons of planetary wave propagation to the upper atmosphere during stratospheric warming events at different QBO phases

Andrey V. Koval [a,*], Nikolai M. Gavrilov [a], Alexander I. Pogoreltsev [b], Elena N. Savenkova [a]

[a] Atmospheric Physics Department, Saint-Petersburg State University, Saint-Petersburg 198504, Russia
[b] Meteorological Forecast Department, Russian State Hydrometeorological University, Saint-Petersburg, Russia

ARTICLE INFO

Keywords:
Middle and upper atmosphere
Planetary waves
Quasi-biennial oscillation
Sudden stratospheric warming
Numerical simulation

ABSTRACT

The dynamical coupling of the lower and upper atmosphere by planetary waves (PWs) is studied. Numerical simulations of planetary wave (PW) amplitudes during composite sudden stratospheric warming (SSW) events in January-February are made using a model of general circulation of the middle and upper atmosphere with initial and boundary conditions typical for the westerly and easterly phases of quasi-biennial oscillation (QBO). The changes in PW amplitudes in the middle atmosphere before, during and after SSW event for the different QBO phases are considered. Near the North Pole, the increase in the mean temperature during SSW reaches 10–30 K at altitudes 30–50 km for four pairs of the model runs with the eQBO and wQBO, which is characteristic for the sudden stratospheric warming event. Amplitudes of stationary PWs in the middle atmosphere of the Northern hemisphere may differ up to 30% during wQBO and eQBO before and during the SSW. After the SSW event SPW amplitudes are substantially larger during wQBO phase. PW refractivity indices and Eliassen-Palm flux vectors are calculated. The largest EP-fluxes in the middle atmosphere correspond to PWs with zonal wavenumber m=1. Simulated changes in PW amplitudes correspond to inhomogeneities of the global circulation, refractivity index and EP-flux produced by the changes in QBO phases. Comparisons of differences in PW characteristics and circulation between the wQBO and eQBO show that PWs could provide effective coupling mechanism and transport dynamical changes from local regions of the lower atmosphere to distant regions of the upper atmosphere of both hemispheres.

1. Introduction

Sudden stratospheric warming (SSW) events significantly influence the formation of weather abnormalities and climate changes in the atmosphere (e.g. Baldwin et al., 2001, 2007; Kuttippurath and Nikulin, 2012). These events may also affect the dynamical and energy processes in the upper atmosphere (Siskind et al., 2010; Kurihara et al., 2010; Liu et al., 2011). Major SSW events imply significant temperature rises (up to 30 K) at altitudes 30–50 km accompanying with corresponding decreases, or even reversals of eastward zonal circulation in the high-latitude stratosphere of the Northern Hemisphere (e.g., Holton, 1975; McIntyre, 1982).

The quasi-biennial oscillations (QBOs) of the zonal mean wind near the equator at stratospheric heights can affect the propagation conditions of planetary waves (e.g. Baldwin et al., 2001; Gavrilov et al., 2015). To eliminate asymmetries in the easterly and westerly wind zones, Pogoreltsev et al. (2014) proposed calculating of differences between monthly mean for each year and climatological (averaged over years 1992–2012) zonal wind velocities near the equator at the altitude of 30 km. This approach is used in the present study.

Gavrilov and Koval (2013) implemented a parameterization of thermal and dynamical effects of orographic gravity waves (OGWs) into the numerical Middle and Upper Atmosphere Model (MUAM) to simulate general circulation at altitudes from the troposphere up to the thermosphere. Gavrilov et al. (2015) studied peculiarities of planetary wave (PW) and OGW interactions in the middle and upper atmosphere at different QBO phases. These simulations showed that dynamical and thermal effects of stationary OGWs could lead to substantial PW amplitude changes up to 50–90%. Transitions from the easterly (eQBO) to the westerly QBO (wQBO) phase can contribute to the PW amplitude changes up to ±30–90% at middle and high northern latitudes. These PW amplitude changes correspond to respective distributions of the Eliassen-Palm fluxes (EP-fluxes) and PW refractivity indices for the different QBO phases.

* Corresponding author.
E-mail address: a.v.koval@spbu.ru (A.V. Koval).

https://doi.org/10.1016/j.jastp.2017.04.013
Received 28 December 2016; Received in revised form 6 April 2017; Accepted 26 April 2017
Available online 27 April 2017

In this study, we continue numerical simulation of global atmospheric circulation for the initial conditions corresponding to the years with westerly and easterly QBO phases. We focus on the changes in amplitudes of stationary planetary waves (SPWs) and westward propagating normal atmospheric modes (NMs) from the Earth's surface up to the lower thermosphere during SSW events for different QBO phases.

2. Atmospheric general circulation model "MUAM"

To research the influence of QBO changes on PW characteristics during SSW events we use the atmospheric general circulation model MUAM (Pogoreltsev, 2007; Pogoreltsev et al., 2007). The model represents the further development of the general circulation model COMMA of Cologne University in Germany (Jakobs et al., 1986). It solves the standard set of primitive equations in spherical coordinates. Calculations in the model include 48 vertical levels at altitudes from the ground up to about 135 km. The regular horizontal model grid has 64 zonal nodes and 36 meridional ones.

In the vertical direction the model uses log-pressure coordinate $z=H^*ln\ (p_0/p)$, where p_0 is the ground pressure and $H=7$ km is the average scale height. In the present simulations, the integration time step is 450 s. The MUAM model can reproduce SPWs and NMs (Pogoreltsev et al., 2014). Low-boundary SPW amplitudes are calculated from the geopotential heights in the lower atmosphere obtained from the UK Met Office stratospheric assimilation data (Swinbank and O'Neill, 1994).

The MUAM involves NM parameterization which uses additional terms in the heat balance equation, having form of time-dependent sinusoidal components with zonal wavenumbers $m=1$ or $m=2$ and periods matching to the simulated NMs. For the latitude structures of NM components, the parameterization uses respective Hough functions, obtained with the method described by Swarztrauber and Kasahara (1985). Periods of NMs are equal to the resonant periods of atmospheric reaction to the wave forcing at low boundary (Pogoreltsev, 1999). The this study we analyzed NMs (1,1), (1,2), (2,1) and (2,2) in notations by Longuet-Higgins (1968), which have periods of 5, 10, 4 and 7 days, respectively. These sources provide amplitudes of simulated NM comparable with the observed ones in the stratosphere (Pogoreltsev et al., 2009).

Low-latitude QBOs are parameterized in the MUAM with additional terms in the momentum equation for zonal velocity. These terms are proportional to differences between calculated and observed zonal mean winds at latitudes 17.5°S – 17.5°N and altitudes 0–50 km. Pogoreltsev et al. (2014) proposed using the differences between monthly mean and climatological (averaged over years 1992–2012) zonal winds at low latitudes and the altitude of 30 km. Westerly and easterly QBO phases correspond to the positive and negative differences. Pogoreltsev et al. (2014) selected ten years with the westerly and ten years with the easterly QBO phases and calculated average for January-February zonal-mean distributions of temperature and zonal wind for both QBO phases. Scaife et al. (2000) showed that records of ten years are enough to capture the reliable climatology of meteorological fields. These distributions are used in the present study.

The numerical simulations start from the initial windless state having a UK Met Office temperature and geopotential height distributions for January - February and performs several steps of adjustment. During the first 30 model days, OGW parameterization in the model is not included and geopotential heights at the lower boundary do not change. After day 31, the observed variations of geopotential are specified. Within the first 120–140 days, the MUAM uses daily averaged heating rates. Pogoreltsev (2007) showed that described procedure allows the model to reach steady-state regime at the end of this time interval. After a day between 120 and 140, daily variations of heating and an additional prognostic equation for the geopotential at the lower boundary are included. The above-mentioned parameterization of NMs is also operates starting from the same day. Starting from the model day 300, seasonal changes in solar heating are triggered, and days 300–390 correspond to December – February. Peculiarities of practical realization of our calculations and initial transition processes were described by Gavrilov et al. (2013) and Koval et al. (2015).

Intra-seasonal variations of the middle atmosphere parameters depend on phases of stratospheric vacillations (e.g., Holton and Mass, 1976). In the MUAM, one can change these phases by altering the day of triggering daily variations of heating during the described above initial adjustment process. To eliminate possible influence of the stratospheric vacillation phase, we made simulations for several MUAM runs with different triggering days of heating daily variations between 120 and 140 at the same initial and climatological data. Then the results were averaged over these ensembles of the MUAM runs separately for eQBO and wQBO.

Our numerical experiments with the MUAM were performed using the initial data sets corresponding to the easterly and westerly QBO phases. We analyzed spatial distributions of PW variations of geopotential height during 11-day intervals before, during, and after the composite SSW events. We estimated increments of amplitudes of SPW modes and westward propagating NMs due to QBO phase change.

3. Results of simulations

In order to study changes in PW characteristics in the middle and upper atmosphere, we considered wave variations of geopotential height during winter season in the Northern Hemisphere. To obtain composite SSW events for the easterly and westerly QBO phases, we simulated two 4-member ensembles of solutions by triggering the diurnal variability of solar heating and prognostic equation for geopotential height at the lower boundary (see Section 2) at different model days between 120 and 140, as it was made by Pogoreltsev et al., (2007, 2009). The triggering NM parameterization on the same days (see Section 2) produces also NM phase shifts at different MUAM runs. Dates of major and minor SWs were obtained using the standard procedure described by Charlton and Polvani (2007), but decreases and reversals of the zonal wind were checked at the pressure level of 10 hPa and above in each MUAM run (an example is shown in Fig. 1). Then we chose three 11-day intervals referred as "before", "during" and "after" the SSW and calculated SPW and NM amplitudes as well as EP-fluxes and refractive indices for each MUAM run and time period separately. After that we obtained averaged over 4 MUAM runs distributions of analyzed PW characteristics and calculated differences between wQBO and eQBO.

Simulations show the existence of minor or major SSW events in each model run at altitudes 20–50 km near the North Pole for described above averaged climatological characteristics.

3.1. Temporal variations of the mean characteristics

The top, middle and bottom panels of Fig. 1 show, respectively, examples of time variations of the simulated amplitude of geopotential height variations produced by PW with $m=1$, zonal mean zonal wind (both at latitude 62°N) and deviation of temperature from its two-month average at latitude 87.5°N. These examples correspond to a pair of the MUAM runs for the easterly and westerly QBO phases (left and right panels of Fig. 1, respectively). The left panels of Fig. 1b and c display increases in temperature at high latitude with respective zonal velocity reversals at altitudes 40–60 km during the middle of February. This behavior corresponds to a stratospheric warming during the easterly QBO phase. On the right panel of Fig. 1c for the westerly QBO phase, one can see the respective warming event with smaller temperature increase, which occurs about 12 days earlier compared to the easterly QBO. The right panel of Fig. 1b reveals weakening of the zonal-mean wind synchronized with the respective increase in the high-latitudinal temperature. Fig. 1a shows significant enhancements of PW amplitude at altitudes above 30 km during the warming events and weakening of the amplitude after the events. Zonal wind velocity recovers up to the original (pre-warming) values after the warming events (see Fig. 1b). In the

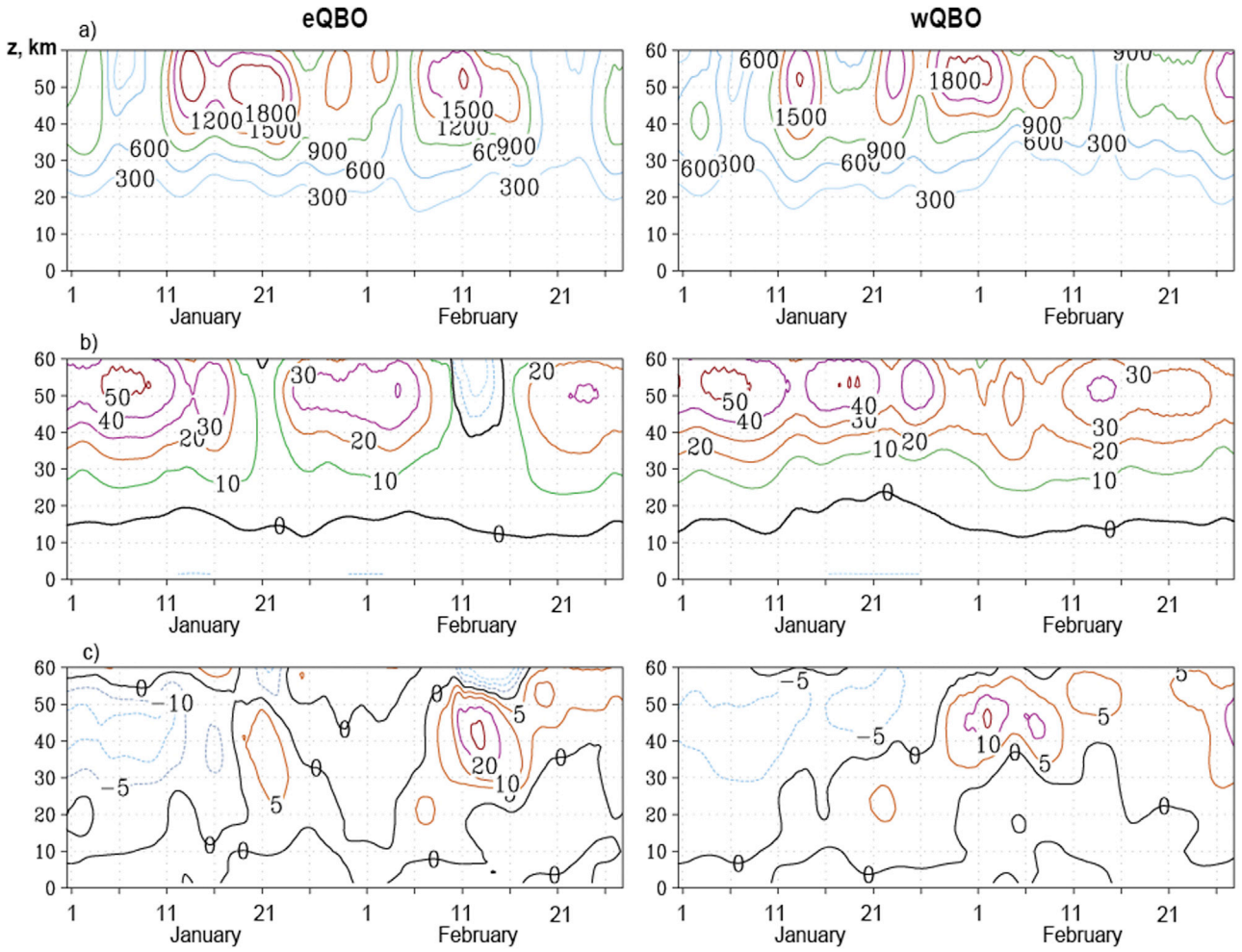

Fig. 1. Time dependence of the geopotential height amplitude (in gpm) of planetary wave with zonal wavenumber m=1 at latitude 62°N (a), zonal mean zonal wind (in m/s) at 62°N (b) and deviation of the mean temperature (in K) at 87.5°N (c) simulated with the MUAM for the easterly and westerly QBO phases (left and right panels, respectively).

left panel of Fig. 1b, the zonal wind velocity becomes smaller after SSW than that before it. This can reflect the seasonal transformation of the general circulation in the middle atmosphere. Comparisons with the UK Met Office stratospheric assimilation data (Swinbank and O'Neill, 1994) showed that the examples of zonal wind and temperature deviations shown in the left and right panels of Fig. 1b and c are similar to the major and minor SSW events observed in the years 2003 and 2002 for the easterly and westerly QBO phases, respectively.

From the distributions similar to Fig. 1 obtained for all four pairs of the MUAM runs, we selected 11-day intervals referred as "before", "during" and "after" the simulated stratospheric warming events, which are given in Table 1. Results of all four pairs of model runs in the MUAM showed that simulated warming events occur 13–20 day earlier during the westerly QBO phase than respective SSWs during the easterly QBO phase. A possible reason could be differences in phases of stratospheric vacillations of the wind and PWs in the middle atmosphere. This can be connected with changes in the global circulation and thermal regime of the middle atmosphere for different QBO phases. Changes in zonal flows near the equator can lead to the changes in global circulation, PW parameters and stratospheric vacillations at all latitudes (e.g., Gavrilov et al., 2015). Similar effects were obtained in other numerical experiments regarding QBO phases (e.g., Holton and Austin, 1990). All other conditions of the MUAM simulation in the present study were equal.

3.2. Planetary wave amplitudes

We analyzed reaction of the global circulation and PWs at altitudes up to the lower thermosphere on the SSW events. SPW and NM amplitudes and phases at different altitudes were obtained using the least squares longitude fitting of hydrodynamic fields simulated with the MUAM. Then

Table 1
Time intervals used for estimations PW parameters and referred as "before", "during" and "after" the composite SSW events simulated for the easterly and westerly QBO phase with the MUAM.

	eQBO			wQBO		
	Before	During	After	Before	During	After
1	6.01–16.01	19.01–29.01	4.02–14.02	21.12–31.12	8.01–18.01	21.01–31.01
2	8.12–18.12	21.12–1.01	4.01–14.01	1.12–11.12	11.12–21.12	23.12–2.01
3	27.01–6.02	9.02–19.02	21.02–3.03	16.01–26.01	29.01–8.02	11.02–21.02
4	7.02–17.02	20.02–2.03	13.03–23.03	5.02–15.02	17.02–27.02	28.02–10.03

differences between SPW and NM amplitudes obtained for the MUAM runs with different QBO phases (wQBO – eQBO) were calculated. Positive differences correspond to larger wave amplitudes during the westerly QBO phase. We estimated amplitudes of SPWs with zonal wavenumbers m=1−4 and of westward propagating NMs having periods τ=5 days and τ=10 days for m=1, also τ=4 days and τ=7 days for m=2.

Fig. 2 represents differences in geopotential height amplitudes of SPWs having zonal wave numbers m=1–4 averaged for 11-day intervals before, during and after the composite SSW event (presented in Table 1) between the MUAM runs for the westerly and easterly QBO phases. To estimate statistical confidence of nonzero differences in SPW amplitudes in Fig. 2, the paired Student's t-test (Rice, 2006) was performed. For each 11-day interval presented in Table 1 at every latitude and altitude, we used for the comparison of 66×64=4224 SPW amplitude pairs at grid nodes in longitude and time (4-h outputs) for each MUAM run. Estimations with the paired t-test showed that the nonzero differences of SPW amplitude have the statistical confidence higher 95%, when their magnitudes are larger than 6–9 gpm, which is satisfied for many regions in

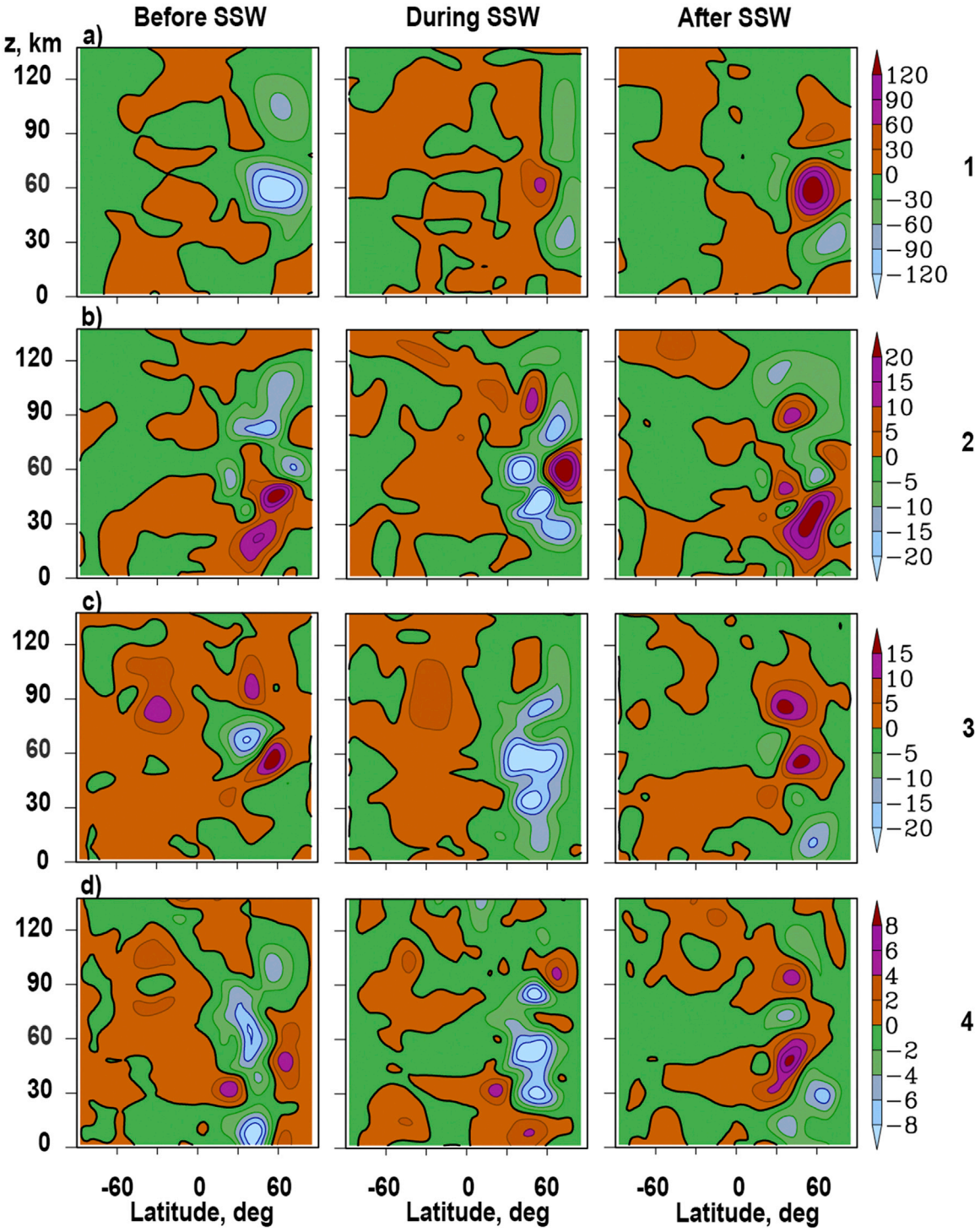

Fig. 2. Differences of the geopotential height amplitudes (in gpm) for SPW modes having zonal wavenumbers m=1, 2, 3, 4 (a, b, c, d) caused by change from wQBO to eQBO phase, averaged for 11-day time intervals before (left), during (middle) and after (right) the simulated SSW events (see Table 1). Thick contours show zero values.

Fig. 2.

Previous simulations with the MUAM showed that during the northern winter SPW1 have larger amplitudes in the Northern Hemisphere. At latitudes 40–70°N, the main maximum is at altitudes 40–60 km and smaller maximum is at 90–110 km (see Fig. 3 by Gavrilov et al., 2015). In the Northern Hemisphere in winter, the background zonal circulation has eastward direction at all altitudes, which may create PW waveguides. The winter average differences in SPW amplitudes between the wQBO and eQBO are mainly negative showing smaller magnitudes of mentioned SPW1 maxima during the westerly QBO phase (Gavrilov et al., 2015). In the left panel of Fig. 2a, our calculations show primarily negative differences (up to 30%) of SPW1 amplitudes at altitudes 40–100 km at middle latitudes before SSW. During the composite warming, the SPW1 amplitude for the wQBO is larger than that for the eQBO at altitudes higher than 40 km, which corresponds to positive differences shown in the middle panel of Fig. 2a. After the SSW, the differences depicted in the right panel of Fig. 2a correspond to generally larger SPW1 amplitudes at altitudes 40–120 km and smaller amplitudes below 40 km for the westerly QBO phase. These differences can indicate changes in PW generation and propagation depending on QBO phase. In our simulations, these changes can partly arise from seasonal changes in the background wind and temperature because SSW events at the eQBO start 13–20 days later (see Table 1).

Fig. 2b reveals the differences between wQBO and eQBO in

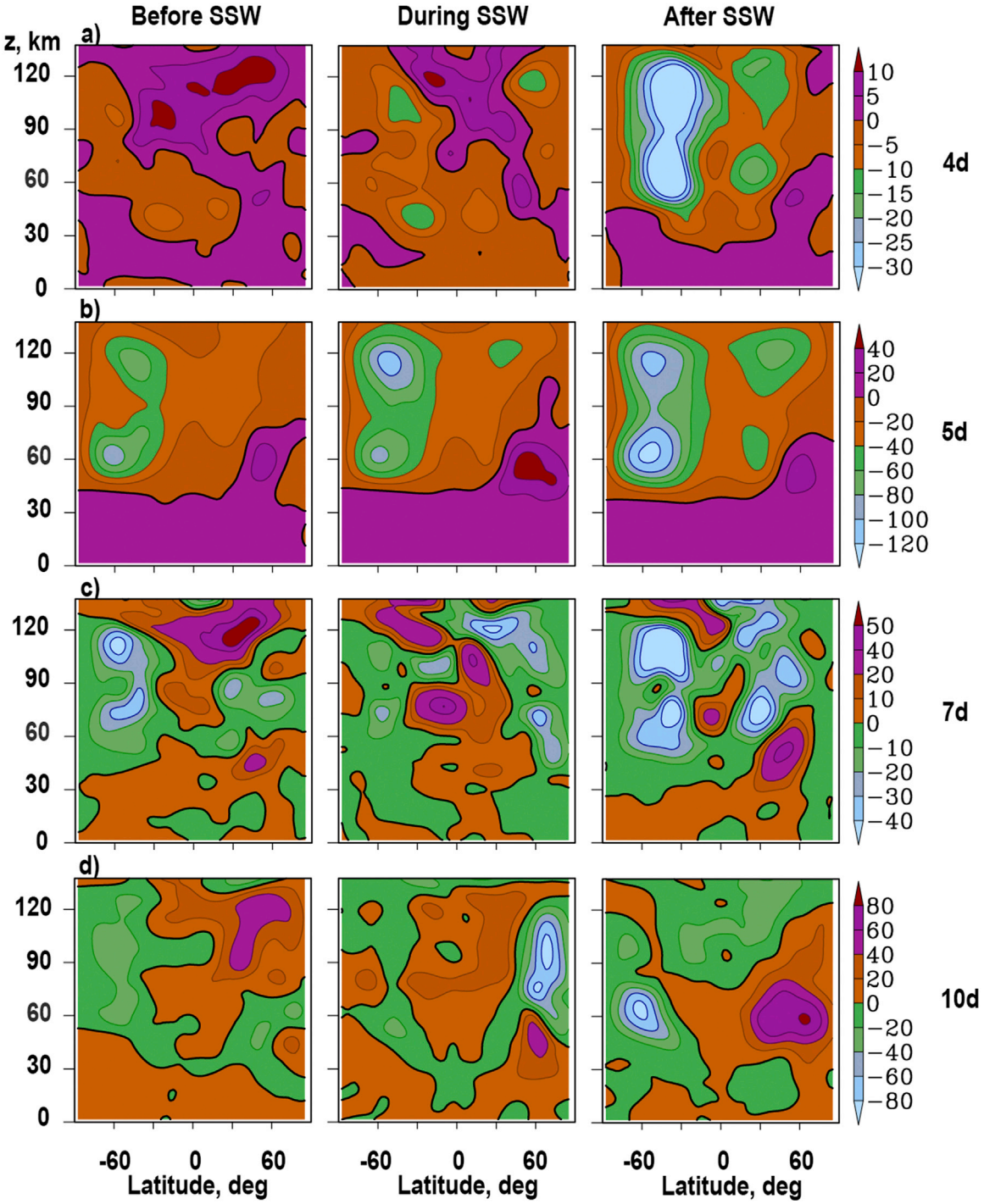

Fig. 3. Same as Fig. 2 but for westward propagating NMs with τ=4 d, m=2 (a); τ=5 d, m=1 (b); τ=7 d, m=2 (c); τ=10 d, m =1 (d).

amplitudes of SPW2 with m=2. According to Fig. 3 given by Gavrilov et al. (2015), the SPW2 amplitude has the main maxima at altitudes 20–40 km, 50–70 km and 90–100 km and latitudes 40−60°N in January – February. SPW2 amplitude differences given in Fig. 2b correspond to enhancements of the two lower maxima (up to 20%) before and after SSW and their weakening during SSW for the wQBO. At altitudes 90–100 km and latitudes 30–60°N, Fig. 2b reveals smaller SPW2 amplitudes before SSW and larger amplitudes during and after SSW for the wQBO. Figs. 2c and 2d show significantly smaller SPW3 and SPW4 amplitudes (up to 15%) at latitudes 30–70°N during SSW and generally larger amplitudes after SSW events for the westerly QBO phase. Variations of SPW amplitudes during SSW may occur due to nonlinear interactions between SPW modes and due to changes in global circulation under easterly and westerly QBO phases. These changes may alter the PW refractivity index and EP-flux considered below.

Fig. 3 depicts the differences in geopotential height amplitudes of westward propagating NMs caused by change from the wQBO to eQBO. The most important features of Fig. 3 are substantial changes of NM amplitudes in the Southern Hemisphere. Amplification of the westward NMs in the Southern (summer) Hemisphere can be conditioned by baroclinic and barotropic instabilities, which was discussed by Liu et al. (2004). Moreover, westward NMs have waveguides for their propagation in the Southern hemisphere (see Section 3.3).

The main alterations in atmospheric circulation at different QBO phases occur in the stratosphere near the equator. Fig. 3 reveals amplitude maxima at low latitudes for 4-, 7- and 10-day NMs increasing at altitudes above 60 km. In addition, one can see substantial amplitude differences at middle and high latitudes of both hemispheres. Amplitudes of many NM modes in Fig. 3 are larger (up to 30%) during the westerly QBO phase at latitudes 40−70°N and altitudes 40–70 km and smaller (up to 20%) above altitudes 60–70 km. At the middle and high latitudes of the southern middle atmosphere, amplitudes are generally smaller (up to 60%) during wQBO for all NM modes. Largest differences between wQBO and eQBO in the Southern Hemisphere in Fig. 3a and b exist for 5- and 4-day NMs, which have largest magnitudes of westward phase speed and better propagation conditions in the westward general circulation of the summer middle atmosphere (see the next section).

Described above significant differences in SPW and NM amplitudes between wQBO and eQBO in both hemispheres can be caused by changes in the general circulation of the middle atmosphere and by respective changes in PW refractivity index and Eliassen-Palm flux, which are discussed in the next chapter. Another important reason of such PW behavior can be the effect of differences in critical line distribution for the SPWs and NMs, which may lead to wave breaking (Liu et al., 2004).

3.3. Eliassen-Palm flux and PW refractivity index

For better understanding PW propagation conditions and changes in wave amplitudes due to change in QBO phases, we calculated the refractivity indexes for SPW and NM modes (e.g., Dickinson, 1968; Matsuno, 1970). We used traditional formulae (e.g., Andrews et al., 1987) to calculate the quasi-geostrophic zonal-mean refractivity index squared, n_m^2, for the PW mode with zonal wavenumber m (see Gavrilov et al., 2015). PWs tend to propagate in atmospheric layers with $n_m^2 > 0$. Considering changes in n_m^2, one can estimate relative importance of the strength, shear, and curvature of the zonal-mean wind for the PW propagation.

The second important PW characteristic is the (EP-flux) vector $\boldsymbol{F_m} = (F_m^{(\varphi)}, F_m^{(z)})$. According to the expression by Andrews et al. (1987), the upward direction of EP-flux indicates the northward wave heat flux, also the southward directed EP-flux indicates the northward PW momentum flux. The divergence of the EP-flux shows the net drag of the zonal-mean flow by PWs. The refractivity index n_m^2 and the EP-flux vector can be used for visualizing the PW propagation conditions.

The refractivity indices and EP-fluxes were calculated for each pair of the MUAM runs and averaged over runs corresponding to eQBO and wQBO phases. Fig. 4 reveals differences between n_m^2 (shaded areas) and EP-fluxes (vectors) for the easterly and westerly QBO phases before, during and after the composite SSW event, for SPWs with m=1−4. Consideration of Fig. 4 shows that the largest differences in n_m^2 for SPWs between wQBO and eQBO occur at altitudes 10–40 km near the equator. There are also n_m^2 differences at the middle and upper latitudes of both hemispheres in Fig. 4 caused by differences in general circulation and thermal regime of the atmosphere during wQBO and eQBO phases. The middle panels of Fig. 4 show smaller n_m^2 values during SSW at the westerly QBO at the middle and high northern latitudes, especially at altitudes higher than 60 km. This corresponds to smaller SPW amplitudes in the middle panels of Fig. 2.

The northern boundary of the region with $n_m^2 > 0$ corresponds to the "critical line", where zonal velocity reaches a critical value prohibiting PW propagation (e.g., Charney and Drazin, 1961; Andrews et al., 1987). Therefore, positive and negative n_m^2 differences in Fig. 4 at high northern latitudes correspond to northward and southward movements of the critical line, which can also influence PW amplitudes and may lead to wave breaking (Liu et al., 2004). Fig. 4 shows also that the vectors of EP-flux differences are generally directed opposite to the EP-vectors at eQBO (see Fig. 5 by Gavrilov et al., 2015). This corresponds to smaller magnitudes of EP-fluxes and smaller SPW amplitudes during the wQBO phase in Fig. 2.

Fig. 5 is similar to Fig. 4 but for the westward propagating NMs. For NMs having stronger amplitudes at low latitudes during the westerly QBO phase (see Fig. 3a, c, d), respective plots of Fig. 5 show a tendency to stronger EP-fluxes directed from sub-equatorial latitudes northward and southward in the Northern and Southern Hemispheres, respectively. This is most noticeable feature in the left panel of Fig. 5c for 7-day NM, at altitudes above 90–100 km before the composite SSW event. Such increased transport of the wave activity may produce larger amplitude of 7-day NM at the mid- and high-latitude upper atmosphere of both hemispheres before SSW during wQBO depicted in the left panel of Fig. 3c. During SSW in the middle panel of Fig. 5c, the northward EP-flux differences in the upper atmosphere become smaller, which corresponds to positive 7-day NM amplitude differences between the wQBO and eQBO in the Southern Hemisphere and negative differences in the Northern Hemisphere at altitudes above 90–100 km in the middle panel of Fig. 5c.

One more source of increased northward EP-fluxes could be region of NM amplitude maxima at latitudes 30–70°N and altitudes 40–70 km, which are noticeable in many panels of Fig. 3. Respective panels of Fig. 5 (especially Fig. 5c and d) show southward-directed EP-flux differences in the regions of these amplitude maxima, which means larger southward EP-fluxes during the westerly QBO phase. An important reason for changes in simulated NM amplitudes at high northern latitudes could be movements of the critical line corresponding to positive and negative differences of n_m^2 in Fig. 5 (see Liu et al., 2004). Due to waveguides for the westward propagating NMs crossing the equator (e.g., Gavrilov et al., 2015), these increased southward EP-fluxes can reach the Southern Hemisphere and change NM amplitudes there. SSW events can modulate these meridional EP-fluxes and lead to changes in NM amplitudes in the Southern Hemisphere (see Fig. 3).

Changes in the EP-fluxes may also occur in the Southern Hemisphere. The right panel of Fig. 5a, b and the middle panel of Fig. 5b show strong northward-downward EP-flux differences at latitudes 30–70°S and altitudes above 90 km for 4- and 5-day NMs. Respective panels of Fig. 4 reveal strong negative NM amplitude differences corresponding to smaller 4- and 5-day wave amplitudes during the westerly QBO phase. The same panels of Fig. 5 show the existence of southward EP-fluxes in the northern upper atmosphere for 4- and 5-day NMs, which can produce transport of PW activity to the Southern Hemisphere. Magnitudes and directions of these EP-fluxes can change at different stages of the composite SSW event (see Fig. 5).

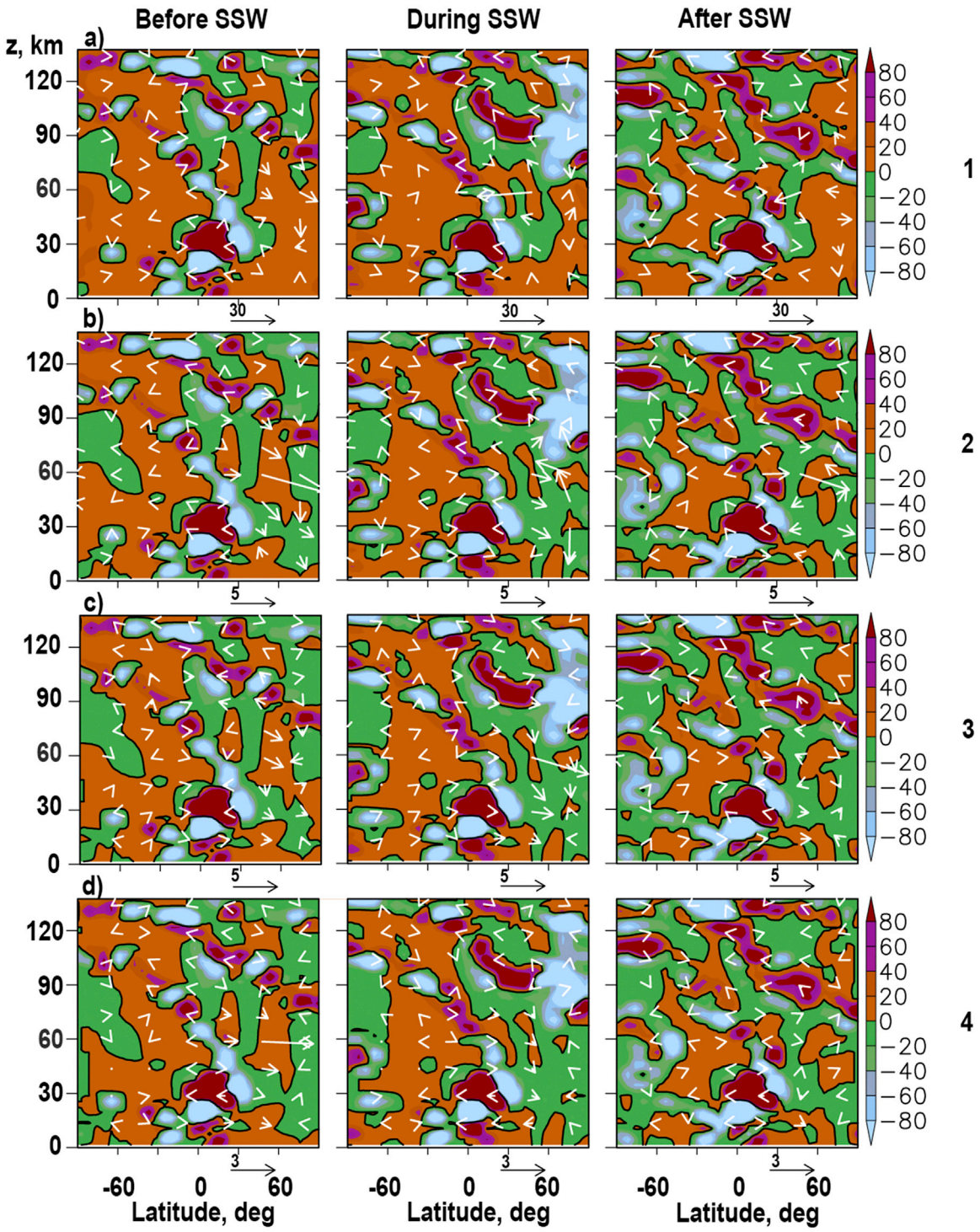

Fig. 4. Differences of normalized refractivity indexes $a^2 n_m^2$ (shading) and specific EP-fluxes in m^3/s^2 (arrows) produced by SPW modes with m=1, 2, 3, 4 (a, b, c, d, respectively) caused by change from wQBO to eQBO phase, averaged for 11-day time intervals before (left), during (middle) and after (right) the simulated SSW events (see Table 1). Thick contours show zero values.

Different atmospheric circulation during the easterly and westerly QBO phases occur near the equator and are parameterized in the MUAM at altitudes 0–50 km (see Section 2). These primary circulation differences may change amplitudes and other characteristics of SPW and NM modes at low latitudes and altitudes. However, the differences in SPW and NM amplitudes between wQBO and eQBO at latitudes from 20°S to 20°N and altitudes 0–50 are generally small in Figs. 2 and 3. Nevertheless, these modified PWs can propagate to higher altitudes and latitudes, interact with other waves and the mean flow, and produce larger differences in PW characteristics and the mean circulation at all latitudes of both hemispheres in the upper atmosphere. Comparisons of differences in PW and circulation between the wQBO and eQBO show that PWs could provide effective coupling mechanism and are capable to transport dynamical changes from local regions of the lower atmosphere to distant regions of the upper atmosphere.

The results of this section show that changes in SPW and NM amplitudes simulated with the MUAM can be connected with differences in the PW refractivity index and EP-flux between the easterly and westerly

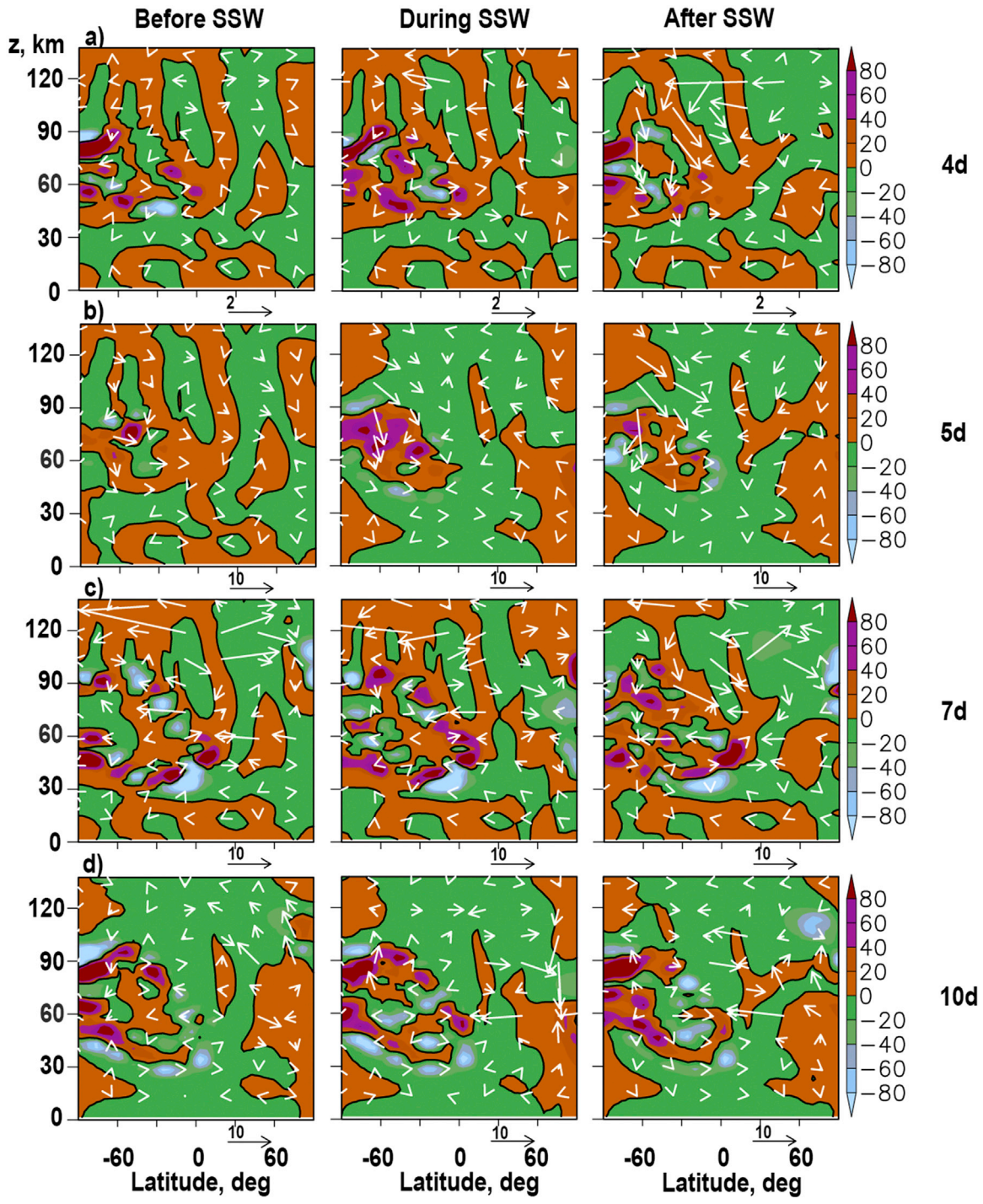

Fig. 5. Same as Fig. 4 but for westward propagating NMs with τ=4 d, m=2 (a); τ=5 d, m=1 (b); τ=7 d, m=2 (c); τ=10 d, m=1 (d).

QBO phases. SSW events can modulate these characteristics and produce respective changes in SPW and NM amplitudes. Cross-equator EP-fluxes can provide dynamical coupling of both hemispheres, especially at high altitudes. Modulation of southward EP-fluxes and their propagation across the equator can cause changes in amplitudes of westward propagating NMs in the Southern Hemisphere during different QBO phases and different SSW stages.

Several of the first years of the interval 1992–2011 used for calculating climatological averages in the present simulations were affected by the cataclysmic eruption of Mount Pinatubo, which occurred in Philippines in June 1991. Effects of the Pinatubo eruption were observed in the stratosphere during several years (McCormick, 1995). We suppose nearly the same Pinatubo influence on stratospheric dynamics during both QBO phases as far as the period of QBO (~2 years) is much smaller than the time interval of the eruption effects in the stratosphere. In addition, used 20-year averaging (10 years for each QBO phase) could substantially diminish the Pinatubo effects. However, it would be useful to make similar simulations for other sets of climatological data.

4. Conclusion

In this study, we performed numerical simulations of planetary wave amplitudes during composite SSW events in January-February for the

conditions typical for the westerly and easterly QBO phases. The numerical simulations employ the MUAM calculating the general circulation of the middle and upper atmosphere using initial and boundary conditions from the UK Met Office stratospheric assimilation data separated to the easterly and westerly QBO phases and averaged over years 1992–2011. We studied differences in PW amplitudes in the middle and upper atmosphere at different stages of composite SSW events for different QBO phases. Events similar to minor and major stratospheric warming at different altitudes were found for each of the MUAM runs and occur 13–20 days earlier during the westerly QBO phase compared to the respective easterly QBO phase SSWs. The differences in SPW and NM amplitudes were averaged over four of the MUAM runs for the each QBO phase creating two 4-members ensembles and compared by choosing 11-day time intervals referred as “before”, “during” and “after” the composite SSW event.

The results of simulation show that differences in SPW amplitudes are larger in the Northern Hemisphere. The amplitude of SPW1 are up to 30% weaker for the wQBO at altitudes 40–70 km at middle latitudes before the SSW. During the SSW, the SPW1 amplitude can increase at altitudes higher than 40 km and become larger for the wQBO than that for the eQBO. After the SSW event, the SPW amplitude becomes generally smaller relative to that during SSW for the both of QBO phases. These peculiarities may be partly associated with average two weeks delay in SSW development in the eQBO compared with the wQBO (see Table 1). This may cause some contribution of the seasonal changes in the atmospheric circulation during the winter-spring season. Variations of SPW amplitudes during SSW may occur due to nonlinear interactions between PW modes and changes in global circulation under the easterly and westerly QBO phases, which produce changes in the refractivity indices for PW modes and the Eliasen-Palm fluxes. Positive differences of SPW amplitudes shown in Fig. 2 correspond frequently to the upward and southward vectors of EP-flux differences. EP-flux changes in the middle and upper atmosphere reflect changes in the wave heat and momentum fluxes, which determines different evolution of SPWs modes.

A remarkable feature of altitude-latitude distributions of amplitudes of westward propagating NM modes is their significant (up to 60%) differences between the eQBO and wQBO in the middle and upper atmosphere of the Southern Hemisphere. In the equatorial area and Northern Hemisphere the differences in the amplitude of 4-day NM reach 20% before and during SSW. Amplitudes of 5-day NM are substantially larger at altitudes below 40 km during and after SSW. Such significant differences of the SPW and NM amplitudes in the Northern Hemisphere due to changes in QBO phases can be connected with changes in displacement of the northern Polar Vortex during SSW events. The largest EP-fluxes in the middle atmosphere are produced by NMs with zonal number m=1.

Our analysis shows that simulated changes in PW amplitudes are associated with modifications of the global circulation, as well as PW refractivity index structures and EP-flux vectors produced by the changes in SSW and QBO phases. Comparisons of differences in PW characteristics and circulation between the wQBO and eQBO show that PWs could provide effective coupling mechanism and are capable to transport dynamical changes from local regions of lower atmosphere to distant regions of the upper atmosphere in both hemispheres.

Acknowledgements

The authors thank the British Atmospheric Data Centre for the access to the UK Met Office stratospheric assimilated data. The improvements of OGW parameterization were supported by the Russian Basic Research Foundation with the research grant 16-35-60013 mol_a_dk. Numerical simulations and their interpreting were supported by the Russian Science Foundation (#14-17-00685).

References

Andrews, D.G., Holton, J.R., Leovy, C.B., 1987. Middle Atmosphere Dynamics. Elsevier, New York.
Baldwin, M.P., Gray, L.J., Dunkerton, T.J., 2001. The quasi-biennial oscillation. Rev. Geophys. 39 (2), 179–229.
Baldwin, M.P., Dameris, M., Shepherd, T.G., 2007. How will the stratosphere affect climate change? Science 316, 1576–1577.
Charlton, A.J., Polvani, L.M., 2007. A new look at stratospheric sudden warmings. Part I: Climatology and modeling benchmarks. J. Clim. 20, 449–469.
Charney, J.G., Drazin, P.G., 1961. Propagation of planetary-scale disturbances from the lower into the upper atmosphere. J. Geophys. Res. 66, 83–109.
Dickinson, R.E., 1968. Planetary Ross by waves propagating vertically through weak westerly wave guides. J. Atmos. Sci. 25, 984–1002.
Gavrilov, N.M., Koval, A.V., 2013. Parameterization of mesoscale stationary orographic wave impact for usage in numerical models of atmospheric dynamics. Izv. Atmos. Ocean. Phys. 49 (3), 243–251.
Gavrilov, N.M., Koval, A.V., Pogoreltsev, A.I., Savenkova, E.N., 2013. Numerical modeling influence of inhomogeneous orographic waves on planetary waves in the middle atmosphere. Adv. Space Res. 51 (11), 2145–2154.
Gavrilov, N.M., Koval, A.V., Pogoreltsev, A.I., Savenkova, E.N., 2015. Simulating influences of QBO phases and orographic gravity wave forcing on planetary waves in the middle atmosphere. Earth Planets Space 67, 86. https://doi.org/10.1186/s40623-015-0259-2.
Holton, J.R., 1975. The dynamic meteorology of the stratosphere and mesosphere. Meteorol. Monogr. 15 (37), 1–218.
Holton, J.R., Mass, C., 1976. Stratospheric vacillation cycles. J. Atmos. Sci. 33 (2218–2215).
Holton, J.R., Austin, J., 1990. The influence of the equatorial QBO on sudden stratospheric warmings. J. Atmos. Sci. 48, 607–618.
Jakobs, H.J., Bischof, M., Ebel, A., Speth, P., 1986. Simulation of gravity wave effects under solstice conditions using a 3-d circulation model of the middle atmosphere. J. Atmos. Terr. Phys. 48, 1203–1223.
Koval, A.V., Gavrilov, N.M., Pogoreltsev, A.I., Savenkova, E.N., 2015. Experiments on Sensitivity of Meridional Circulation and Ozone Flux to Parameterizations of Orographic Gravity Waves and QBO Phases in A General Circulation Model of the middle atmosphere Geoscientific Model Development Discussions, 8(7), pp. 5643–5670. ⟨http://doi.org/10.5194/gmdd-8-5643-2015⟩.
Kurihara, J., Ogawa, Y., Oyama, S., Nozawa, S., Tsutsumi, M., Hall, C.M., Tomikawa, Y., Fujii, R., 2010. Links between a stratospheric sudden warming and thermal structures and dynamics in the high-latitude mesosphere, lower thermosphere, and ionosphere. Geophys. Res. Lett. 37, L13806. https://doi.org/10.1029/2010GL043643 (2010).
Kuttippurath, J., Nikulin, G., 2012. A comparative study of the major sudden stratospheric warmings in the Arctic winters 2003/2004–2009/2010. Atmos. Chem. Phys. 12, 8115–8129.
Liu, H., Doornbos, E., Yamamoto, M., Ram, S.T., 2011. Strong thermospheric cooling during the 2009 major stratosphere warming. Geophys. Res. Lett. 38, L12102. https://doi.org/10.1029/2011GL047898.
Liu, H.-L., Talaat, E.R., Roble, R.G., Lieberman, R.S., Riggin, D.M., Yee, J.-H., 2004. The 6.5-day wave and its seasonal variability in the middle and upper atmosphere. J. Geophys. Res. 109, D21112. https://doi.org/10.1029/2004JD004795.
Longuet-Higgins, M.S., 1968. The eigenfunctions of Laplace’s tidal equation over a sphere. Philos. Trans. R. Soc. Lond. 262, 511–607.
Matsuno, T., 1970. Vertical propagation of stationary planetary waves in the winter Northern Hemisphere. J. Atmos. Sci. 27, 871–883.
McCormick, P., Thomason, L.W., Trepte, Ch.R., 1995. Atmospheric effects of the Mt Pinatubo eruption. Nature 373 (6513), 399–404.
McIntyre, M.E., 1982. How well do we understand the dynamics of stratospheric warmings. J. Meterol. Soc. Jpn. 60, 37–64.
Pogoreltsev, A.I., 1999. Simulation of planetary waves and their influence on the zonally averaged circulation in the middle atmosphere. Earth Planets Space 51 (7/8), 773–784.
Pogoreltsev, A.I., 2007. Generation of normal atmospheric modes by stratospheric vacillations. Izv. Atmos. Ocean. Phys. 43 (4), 423–435.
Pogoreltsev, A.I., Savenkova, E.N., Pertsev, N.N., 2014. Sudden stratospheric warmings: the role of normal atmospheric modes. Geomagn. Aeron. 54 (3), 357–372.
Pogoreltsev, A.I., Vlasov, A.A., Froehlich, K., Jacobi, Ch, 2007. Planetary waves in coupling the lower and upper atmosphere. J. Atmos. Sol.-Terr. Phys. 69, 2083–2101. https://doi.org/10.1016/j.jastp.2007.05.014.
Pogoreltsev, A.I., Kanukhina, A., Yu, Suvorova, E.V., Savenkova, E.N., 2009. Variability of planetary waves as a signature of possible climatic. Change J. Atmos. Sol.-Terr. Phys. 71, 1529–1539. https://doi.org/10.1016/j.jastp.2009.05.011.
Rice, J.A., 2006. Mathematical Statistics and Data Analysis, 3rd ed. Duxbury Press, Belmont.
Scaife, A.A., Austin, J., Butchart, N., Pawson, S., Keil, M., Nash, J., James, I.N., 2000. Seasonal and in-terannual variability of the stratosphere diagnosed from UKMO TOVS analysis. Q. J. R. Meteorol. Soc. 126, 2585–2604.
Siskind, D.E., Eckermann, S.D., McCormack, J.P., Coy, L., Hoppel, K.W., Baker, N.L., 2010. Case studies of the mesospheric response to recent minor, major and extended stratospheric warmings. J. Geophys. Res. 115 https://doi.org/10.1029/2010JD014114.
Swarztrauber, P.N., Kasahara, A., 1985. The vector harmonic analysis of Laplace’s tidal equations. SIAM J. Sci. Stat. Comput. 6, 464–491.
Swinbank, R., O’Neill, A., 1994. Stratosphere-troposphere assimilation system. Mon. Weather Rev. 122, 686–702.